Speckle Reducing Anisotropic Diffusion

Yongjian Yu and Scott T. Acton, *Senior Member, IEEE*

***Abstract*—This paper provides the derivation of speckle reducing anisotropic diffusion (SRAD), a diffusion method tailored to ultrasonic and radar imaging applications. SRAD is the edge-sensitive diffusion for speckled images, in the same way that conventional anisotropic diffusion is the edge-sensitive diffusion for images corrupted with additive noise. We first show that the Lee and Frost filters can be cast as partial differential equations, and then we derive SRAD by allowing edge-sensitive anisotropic diffusion within this context. Just as the Lee and Frost filters utilize the coefficient of variation in adaptive filtering, SRAD exploits the *instantaneous* coefficient of variation, which is shown to be a function of the local gradient magnitude and Laplacian operators. We validate the new algorithm using both synthetic and real linear scan ultrasonic imagery of the carotid artery. We also demonstrate the algorithm performance with real SAR data. The performance measures obtained by means of computer simulation of carotid artery images are compared with three existing speckle reduction schemes. In the presence of speckle noise, speckle reducing anisotropic diffusion excels over the traditional speckle removal filters and over the conventional anisotropic diffusion method in terms of mean preservation, variance reduction, and edge localization.**

***Index Terms*—Anisotropic diffusion, image enhancement, speckle reduction, ultrasound imaging.**

I. Introduction

SPECKLE, a form of multiplicative, locally correlated noise, plagues imaging applications such as medical ultrasound image interpretation. For images that contain speckle, a goal of enhancement is to remove the speckle without destroying important image features. In certain applications, however, the removal of speckle may be counterproductive. Examples in which speckle *preservation* is important include feature tracking in ultrasonic imaging [19] and detection of features that are of the same scale as the speckle patterns (e.g., coagulation damage) [18]. In cases where speckle removal is desired (e.g., region-based detection, segmentation, and classification) [17], [21]–[23], the speckle reducing filters have originated mainly in the synthetic aperture radar (SAR) community. The most widely cited and applied filters in this category include the Lee [9]–[11], Frost [6], Kuan [8], and Gamma MAP filters [12].

The Lee and Kuan filters have the same formation, although the signal model assumptions and the derivations are different. Essentially, both the Lee and Kuan filters form an output image by computing a linear combination of the center pixel intensity in a filter window with the average intensity of the window. So, the filter achieves a balance between straightforward averaging (in homogeneous regions) and the identity filter (where edges and point features exist). This balance depends on the coefficient of variation inside the moving window.

The Frost filter also strikes a balance between averaging and the all-pass filter. In this case, the balance is achieved by forming an exponentially shaped filter kernel that can vary from a basic average filter to an identity filter on a pointwise, adaptive basis. Again, the response of the filter varies locally with the coefficient of variation. In case of low coefficient of variation, the filter is more average-like, and in cases of high coefficient of variation, the filter attempts to preserve sharp features by not averaging.

More recently, the Gamma maximum *a posteriori* (MAP) and extended versions of the Lee filter and the Frost filter have been introduced to alter performance locally according to three cases [12], [13]. In the first case, pure averaging is induced when the local coefficient of variation is below a lower threshold. Above a higher threshold, the filter performs as a strict all-pass (identity) filter. When the coefficient of variation exists in between the two thresholds, a balance between averaging and the identity is computed (as with the standard Lee and Frost filters).

Although the existing despeckle filters are termed as "edge preserving" and "feature preserving," there exist major limitations of the filtering approach. First, the filters are sensitive to the size and shape of the filter window. Given a filter window that is too large (compared to the scale of interest), over-smoothing will occur and edges will be blurred. A small window will decrease the smoothing capability of the filter and will leave speckle. In terms of window shape, a square window (as is typically applied) will lead to corner rounding of rectangular features that are not oriented at perfect 90° rotations, for example. Second, the existing filters do not enhance edges—they only inhibit smoothing near edges. When any portion of the filter window contains an edge, the coefficient of variation will be high and smoothing will be inhibited. Therefore, noise/speckle in the neighborhood of an edge (or in the neighborhood of a point feature with high contrast) will remain after filtering. Third, the despeckle filters are not directional. In the vicinity of an edge, all smoothing is precluded, instead of inhibiting smoothing in directions perpendicular to the edge and encouraging smoothing in directions parallel to the edge. Last, the thresholds used in the enhanced filters, although motivated by statistical arguments, are *ad hoc* improvements that only demonstrate the insufficiency of the window-based approaches. The hard thresholds that enact neighborhood averaging and identity filtering in the extreme cases lead to blotching artifacts from averaging filtering and noisy boundaries from leaving the sharp features unfiltered.

Manuscript received August 9, 2001; revised June 24, 2002. The associate editor coordinating the review of this manuscript and approving it for publication was Dr. Nasser Kehtarnavaz.

The authors are with the Department of Electrical and Computer Engineering, University of Virginia, Charlottesville, VA 22904 USA (e-mail: yy6b@virginia.edu; acton@virginia.edu).

Digital Object Identifier 10.1109/TIP.2002.804276

1057-7149/02$17.00 © 2002 IEEE

In this paper, we have outlined a partial differential equation (PDE) approach to speckle removal that we call speckle reducing anisotropic diffusion (SRAD). The PDE-based speckle removal approach allows the generation of an image scale space (a set of filtered images that vary from fine to coarse) without bias due to filter window size and shape. SRAD not only preserves edges but also enhances edges by inhibiting diffusion across edges and allowing diffusion on either side of the edge. SRAD is adaptive and does not utilize hard thresholds to alter performance in homogeneous regions or in regions near edges and small features. The new diffusion technique is based on the same minimum mean square error (MMSE) approach to filtering as the Lee (Kuan) and Frost filters. In fact, we show that the SRAD can be related directly to the Lee and Frost window-based filters. So, SRAD is the edge sensitive extension of conventional adaptive speckle filter, in the same manner that the original Perona and Malik anisotropic diffusion [15] is the edge sensitive extension of the average filter. In this sense, we extend the application of anisotropic diffusion to applications such as radar and medical ultrasound in which signal-dependent, spatially correlated multiplicative noise is present.

The paper is organized as follows. In Section II, we first review nonlinear anisotropic diffusion and the current speckle filtering techniques. Then, we establish the relationship between SRAD and the speckle filters. In Section III, we describe the proposed strategy for extending nonlinear anisotropic diffusion for imagery corrupted by speckle and derive SRAD. Section IV defines the criteria for quantifying the performance of the proposed algorithm and presents experimental results for synthetic and real ultrasound images of human carotid artery. We also demonstrate the possible application of SRAD to radar imaging. In Section V, we conclude the paper.

II. Anisotropic Diffusion vs. Adaptive Speckle Filter

A. Anisotropic Diffusion

Perona and Malik [15] proposed the following nonlinear PDE for smoothing image on a continuous domain:

$$\begin{cases} \dfrac{\partial I}{\partial t} = div[c(|\nabla I|) \cdot \nabla I] \\ I(t=0) = I_0 \end{cases} \tag{1}$$

where ∇ is the gradient operator, div the divergence operator, $|\,|$ denotes the magnitude, $c(x)$ the diffusion coefficient, and I_0 the initial image. They suggested two diffusion coefficients

$$c(x) = \frac{1}{1+(x/k)^2} \tag{2}$$

and

$$c(x) = \exp[-(x/k)^2] \tag{3}$$

where k is an edge magnitude parameter.

In the anisotropic diffusion method, the gradient magnitude is used to detect an image edge or boundary as a *step* discontinuity in intensity. If $|\nabla I| \gg k$, then $c(|\nabla I|) \to 0$, and we have an all-pass filter; if $|\nabla I| \ll k$, then. $c(|\nabla I|) \to 1$, and we achieve isotropic diffusion (Gaussian filtering).

A discrete form of (1) is given by

$$I_s^{t+\Delta t} = I_s^t + \frac{\Delta t}{|\overline{\eta}_s|} \sum_{p \in \overline{\eta}_s} c(\nabla I_{s,p}^t) \nabla I_{s,p}^t \tag{4}$$

where I_s^t is the discretely sampled image, s denotes the pixel position in a discrete two-dimensional (2-D) grid, and Δt is the time step size, $\overline{\eta}_s$ represents the spatial neighborhood of pixel s, $|\overline{\eta}_s|$ is the number of pixels in the window (usually four, except at the image boundaries), and $\nabla I_{s,p}^t = I_p^t - I_s^t, \forall p \in \overline{\eta}_s$.

The advantages of anisotropic diffusion include intra-region smoothing and edge preservation. Anisotropic diffusion performs well for images corrupted by additive noise. Several enhancements and edge detection methods have been described in the literature [3] for images with additive noise. In cases where images contain speckle, anisotropic diffusion will actually *enhance* the speckle, instead of eliminating the corruption. The work of this paper uses the strengths of the PDE approach to produce edge-sensitive speckle reduction.

B. Adaptive Speckle Filters

In this section, we briefly describe the speckle reducing filters: the Lee filter and the Frost filter. Then, we examine the relationship between the speckle filters and the diffusion technique.

1) Lee Filter [9]: The Lee filter is designed to eliminate speckle noise while preserving edges and point features in radar imagery. Based on a linear speckle noise model and the minimum mean square error (MMSE) design approach, the filter produces the enhanced data according to

$$\hat{I}_s = \overline{I}_s + k_s \left(I_s - \overline{I}_s\right) \tag{5}$$

where $\overline{I}_s$ is the mean value of the intensity within the filter window η_s; and k_s is the adaptive filter coefficient determined by

$$k_s = 1 - C_u^2/C_s^2. \tag{6}$$

Here,

$$C_s^2 = (1/|\eta_s|) \sum_{p \in \eta} \left(I_p - \overline{I}_s\right)^2 \Big/ \left(I_p - \overline{I}_s\right)^2 \tag{7}$$

and C_u^2 is a constant for a given image and can be determined by either

$$C_u^2 = 1/ENL \tag{8}$$

or

$$C_u^2 = \frac{\mathrm{var}(z')}{(\overline{z}')^2} \tag{9}$$

where ENL is the effective number of looks of the noisy image, $\mathrm{var}(z')$ and $\overline{z}'$ are the intensity variance and mean over a homogeneous area of the image, respectively.

The local statistic C_s plays an essential role in controlling the filter: if $C_s \to C_u$, then $k_s \to 0$, and, if $C_s \to \infty$, then $k_s \to 1$. In general, the value of k_s approaches zero in uniform areas, leading to the same result as that of the mean filter. On the

other hand, the value of k_s approaches unity at edges, resulting in little modification to the pixel values near edges.

2) Frost Filter [6]: The Frost filter uses an exponentially damped convolution kernel that adapts to regions containing edges by exploiting local statistics. The filter output is determined by

$$\hat{I}_s = \sum_{p \in \eta_s} m_p I_p \tag{10}$$

where

$$m_p = \exp(-KC_s^2 d_{s,p}) \Big/ \sum_{p \in \eta} \exp(-KC_s^2 d_{s,p}) \tag{11}$$

$$d_{s,p} = \sqrt{(i-i_p)^2 + (j-j_p)^2} \tag{12}$$

where K is the damping factor, (i, j) are the grid coordinates of pixel s, and (i_p, j_p) are those of pixel p.

The factor K is chosen such that when in a homogeneous region KC_s^2 approaches zero, yielding the mean filter output; at an edge KC_s^2 becomes so large that filtering is inhibited completely.

C. Relationship of the Lee and Frost Filters With Diffusion

1) Lee Filter and Diffusion: Typically, the Lee filter operates in a 7×7 moving window. Now let us choose the filter window as $\eta_s = \overline{\eta}_s \equiv \{(i-1, j), (i, j-1), (i+1, j), (i+1, j)\}$ at an interior site $s = (i, j)$.

We can express the special case of the Lee filter with window $\overline{\eta}_s$in the following form:

$$\begin{aligned}\hat{I}_{i,j} &= I_{i,j} + (1-k_{i,j})\left(\overline{I}_{i,j} - I_{i,j}\right)\\ &= I_{i,j} + (1-k_{i,j})\left(\frac{1}{|\overline{\eta}_s|}\sum_{p\in\overline{\eta}_s} I_p - I_{i,j}\right)\\ &= I_{i,j} + (1-k_{i,j})\left(\frac{1}{|\overline{\eta}_s|}\sum_{p\in\overline{\eta}_s} (I_p - I_{i,j})\right)\\ &= I_{i,j} + (1-k_{i,j})\frac{1}{|\overline{\eta}_s|}\nabla^2 I_{i,j}\end{aligned} \tag{13}$$

where $|\overline{\eta}_s|$ (=4) is the number of pixels in the window.

Substituting $I_{i,j}^{t+1}, I_{i,j}^t, k_{i,j}^t$ for $\hat{I}_{i,j}, I_{i,j}, k_{i,j}$ in (13), respectively, we obtain

$$I_{i,j}^{t+1} = I_{i,j}^t + (1-k_{i,j}^t)\frac{1}{|\overline{\eta}_s|}\nabla^2 I_{i,j}^t. \tag{14}$$

Comparing (14) with (4) and noting the equality

$$\begin{aligned}\nabla^2 I_{i,j} &= I_{i+1,j} + I_{i-1,j} + I_{i,j+1} + I_{i,j-1} - 4I_{i,j}\\ &= \sum_{p\in\overline{\eta}_s}(I_p - I_{i,j})\end{aligned} \tag{15}$$

we show that the form of (14) is a special case of (4) in which $c(\,)$ can be taken out of the summation and $\Delta t = 1$. In other words, the Lee filter can be posed as a discrete *isotropic* diffusion equation.

Moreover, it is interesting to show the effect of assigning slightly different weights to the four directional differences in (14) such that

$$\begin{aligned}\hat{I}_{i,j} = I_{i,j} + \frac{1}{|\overline{\eta}_s|}[&(1-k_{i+1,j})(I_{i+1,j} - I_{i,j})\\ &+ (1-k_{i,j})(I_{i-1,j} - I_{i,j})\\ &+ (1-k_{i,j+1})(I_{i,j+1} - I_{i,j})\\ &+ (1-k_{i,j})(I_{i,j-1} - I_{i,j})].\end{aligned} \tag{16}$$

In fact, (16) reduces to

$$\hat{I}_{i,j} = I_{i,j} + \frac{1}{|\overline{\eta}_s|}\, div[(1-k_{i,j})\nabla I_{i,j}]. \tag{17}$$

With variable substitutions in (17), we immediately recognize that (17) is a form of anisotropic diffusion [as in (4)] where $\Delta t = 1$.

The Lee filter and enhanced Lee filter [12] process a current pixel based on its intensity and the intensities of neighboring pixels inside a fixed square window. Thus, these two filters have no mechanism to enhance edges or feature structures within a window. The modification of the Lee filter to include directional sensitivity and filtering perpendicular to the edge direction would significantly enhance the ability to remove the speckle in the vicinity of edges and small features. That is what refined Lee filter [10] does. Similarly, with (17) the diffusion assumes sort of edge directional sensitivity.

2) Frost Filter and Diffusion: Let the filter window be chosen as $\eta_s = \overline{\eta}_s$. Thus, we have from (12) that $d_{s,p} = 1$ $\forall p \in \overline{\eta}_s$, which implies that $m_p = 1/|\overline{\eta}_s|$ for any $p \in \overline{\eta}_s$. The Frost filter (10) is reduced, in this case, to

$$\begin{aligned}\hat{I}_{i,j} &= \frac{1}{|\overline{\eta}_s|}\sum_{p\in\overline{\eta}_s} I_p = I_{i,j} + \frac{1}{|\overline{\eta}_s|}\sum_{p\in\overline{\eta}_s}(I_p - I_{i,j})\\ &= I_{i,j} + \frac{1}{|\overline{\eta}_s|}\nabla^2 I_{i,j}\end{aligned} \tag{18}$$

which resembles the form of the isotropic diffusion update function with $\Delta t = 1$.

If we reassign weights in (10) such that

$$\hat{I}_{i,j} = \frac{M_{i+1,j}I_{i+1,j} + M_{i,j}I_{i-1,j} + M_{i,j+1}I_{i,j+1} + M_{i,j}I_{i,j-1}}{M_{i+1,j} + M_{i,j} + M_{i,j+1} + M_{i,j}} \tag{19}$$

where $M_{i,j} = \exp(-KC_{i,j}^2)$, we can reorganize (19) as shown in (20) at the bottom of the next page, where $K_0' = ((M_{i+1,j} + M_{i,j+1} + 2M_{i,j})/4)^{-1}$.

Substituting $I_{i,j}^{t+\Delta t}, I_{i,j}^t, k_{i,j}^t$ for $\hat{I}_{i,j}, I_{i,j}, k_{i,j}$, respectively, and letting $\Delta t = K_0'$ (its value is between 0 and 1), we show (20) is in the form of (4) where Δt is space-and-time varying. So, both the Lee and Frost filters resemble isotropic diffusion processes and can be modified to enact anisotropic diffusion. These observations lead to the construction of speckle reducing anisotropic diffusion.

III. Speckle Reducing Anisotropic Diffusion

Casting the Lee and Frost filters in the framework of the PDE bridges and unifies two seemingly different methods: the PDE

approach and the adaptive filtering approach. Perhaps more importantly, the framework allows us to develop a new model for speckle reduction, which may open new avenues for processing ultrasound and radar images. In this section, we derive the speckle reducing anisotropic diffusion (SRAD) method.

A. Coefficient of Variation

Until now, our focus has been on the similarity between the conventional adaptive despeckle filters and anisotropic diffusion. By extending the PDE versions of the despeckle filters, we have formulized a more general update function

$$I_{i,j}^{t+\Delta t} = I_{i,j}^{t} + \frac{\Delta t}{|\overline{\eta}_s|}\, div[c(C_{i,j}^{t})\nabla I_{i,j}^{t}] \tag{21}$$

where $c(\cdots)$ is a bounded nonnegative decreasing function. As with conventional anisotropic diffusion, $c(\cdots)$ is the diffusion coefficient.

In discussing the background on the Lee and Frost filters, we have noted the importance of the local statistic $C_{i,j}$, the coefficient of variation, in speckle filtering. To derive a PDE version of the classical speckle reducing filters, we must examine the coefficient of variation in conjunction with developing a diffusion coefficient $c(\cdots)$ that inhibits smoothing at the edges. Specifically, we need to derive a discretized version of the coefficient of variation that is applicable to PDE evolution. In a sense, this function can be called an "instantaneous coefficient of variation." This subsection develops such an operator.

First, we write the local variance estimate of intensity in $\overline{\eta}_s$ as

$$\frac{1}{|\overline{\eta}_s|}\sum_{p\in\overline{\eta}_s}\left(I_p - \overline{I}_{i,j}\right)^2 = \overline{(I^2)}_{i,j} - \left(\overline{I}_{i,j}\right)^2 \tag{22}$$

where $\overline{(I^2)}_{i,j}$ is the average of intensity squared at position (i, j). Then, we express the local intensity mean and local intensity squared mean estimates in terms of Laplacian as follows:

$$\begin{aligned}\overline{I}_{i,j} &= I_{i,j} + \overline{I}_{i,j} - I_{i,j} = I_{i,j} + \frac{1}{|\overline{\eta}_s|}\sum_{p\in\overline{\eta}_s}(I_p - I_{i,j})\\ &= I_{i,j} + \frac{1}{|\overline{\eta}_s|}\nabla^2 I_{i,j} \qquad (23)\\ \overline{(I^2)}_{i,j} &= (I^2)_{i,j} + (1/|\overline{\eta}_s|)\nabla^2 (I^2)_{i,j}. \qquad (24)\end{aligned}$$

Substituting first (23) and (24) into (22) and then substituting the result and (23) into (7), we have

$$C_{i,j}^2 = \frac{\left[I_{i,j}^2 + \frac{1}{|\overline{\eta}_s|}\nabla^2 I_{i,j}^2\right]}{\left[I_{i,j} + \frac{1}{|\overline{\eta}_s|}\nabla^2 I_{i,j}\right]^2} - 1. \tag{25}$$

In the continuous domain, we have the following equality:

$$\nabla^2 I^2 = 2|\nabla I|^2 + 2I\nabla^2 I. \tag{26}$$

On the discrete 2-D grid, (26) can be represented by

$$\nabla^2 I_{i,j}^2 = |\nabla_L I_{i,j}|^2 + |\nabla_R I_{i,j}|^2 + 2I_{i,j}\nabla^2 I_{i,j} \tag{27}$$

where $\nabla_L I_{i,j}$ and $\nabla_R I_{i,j}$, two difference approximations to the gradient, are given by

$$\nabla_L I_{i,j} = [I_{i,j} - I_{i-1,j},\, I_{i,j} - I_{i,j-1}] \tag{28}$$

$$\nabla_R I_{i,j} = [I_{i+1,j} - I_{i,j},\, I_{i,j+1} - I_{i,j}]. \tag{29}$$

Allowing $|\nabla I_{i.j}|^2$ to be discretized as the average of $|\nabla_L I_{i,j}|^2$ and $|\nabla_R I_{i,j}^2|$, and substituting (27) into (25), we obtain the following form for $C_{i,j}^2$:

$$C_{i,j}^2 = \frac{\frac{1}{2}|\nabla I_{i,j}|^2 - \frac{1}{16}(\nabla^2 I_{i,j})^2}{\left[I_{i,j} + \frac{1}{4}\nabla^2 I_{i,j}\right]^2}. \tag{30}$$

It is required that $C_{i,j} \geq 0$. Although by the derivation of (30) its numerator is nonnegative, the denominator of (30) may become zero at some points if we do not impose some restriction on the image function.

Proposition I: If $I_{i,j} > 0$ everywhere over a 2-D coordinate grid Ω, then (30) is well defined over Ω.

Proof: We only need to show that the denominator of (30) cannot be zero if $I_{i,j} > 0$ everywhere. Suppose that the denominator of (30) becomes zero at position (i, j). Then,

$$\begin{aligned}\nabla^2 I_{i,j} = -4I_{i,j}. &\Rightarrow I_{i+1,j} + I_{i-1,j} + I_{i,j-1} + I_{i,j+1} - 4I_{i,j}\\ = -4I_{i,j}. &\Rightarrow I_{i+1,j} + I_{i-1,j} + I_{i,j-1} + I_{i,j+1} = 0.\end{aligned}$$

But, by assumption, $I_{i,j} > 0$ for all $(i, j) \in \Omega$. So, it is not possible for the denominator of (30) to be zero.

We denote the special case of $C_{i,j}$, one that is computed over $\overline{\eta}_s$, by $q_{i,j}$ for convenience and assume that the image intensity function has no zero point over its support. So, $q_{i,j}$ can be viewed as a discretization of

$$q = \sqrt{\frac{\frac{1}{2}\left(\frac{|\nabla I|}{I}\right)^2 - \frac{1}{4^2}\left(\frac{\nabla^2 I}{I}\right)^2}{\left[1 + \frac{1}{4}\left(\frac{\nabla^2 I}{I}\right)\right]^2}} \tag{31}$$

$$\begin{aligned}\hat{I}_{i,j} &= I_{i,j} + \frac{M_{i+1,j}I_{i+1,j} + M_{i,j}I_{i-1,j} + M_{i,j+1}I_{i,j+1} + M_{i,j}I_{i,j-1}}{M_{i+1,j} + M_{i,j} + M_{i,j+1} + M_{i,j}} - I_{i,j}\\ &= I_{i,j} + \frac{M_{i+1,j}(I_{i+1,j} - I_{i,j}) + M_{i,j}(I_{i-1,j} - I_{i,j}) + M_{i,j+1}(I_{i,j+1} - I_{i,j}) + M_{i,j}(I_{i,j-1} - I_{i,j})}{M_{i+1,j} + M_{i,j} + M_{i,j+1} + M_{i,j}}\\ &= I_{i,j} + \frac{K_0'}{|\overline{\eta}_s|}\, div[M_{i,j}\nabla I_{i,j}] \qquad (20)\end{aligned}$$

over a uniform grid of unit step size in two directions.

As $C_{i,j}$ is usually called local coefficient of variation, we call the function q the *instantaneous coefficient of variation*. It combines a normalized gradient magnitude operator and a normalized Laplacian operator to act like an edge detector for speckled imagery. High relative gradient magnitude and low relative Laplacian tend to indicate an edge. At the center of an edge, the Laplacian term undergoes zero crossing and the gradient term dominates, resulting in $q_{i,j} \to |\nabla I_{i,j}|/I_{i,j}$. The *instantaneous coefficient of variation* allows for edge detection in bright regions as well as in dark regions.

So, the original anisotropic diffusion algorithm [15] may be viewed as the edge-sensitive PDE extension of the Gaussian-weighted averaging filter. In the same way, SRAD may be viewed as the edge sensitive PDE version of the conventional adaptive speckle reducing filters. With SRAD, the instantaneous coefficient of variation plays a crucial role as an edge detector in the presence of speckle. In the following section, we show how the instantaneous coefficient of variation, q, is incorporated in the speckle reducing diffusion technique.

To end this subsection, we present the second proposition.

Proposition II: Given an initial image $\{I^0_{i,j}\}$ having finite power and no zero points over domain Ω, the diffusion process (21) can be updated such that $\{I^t_{i,j}\}$ have no zero points over Ω.

Proof: Step 1. Since $I^0_{i,j}$ is nonzero everywhere, $q^0_{i,j}$ is well defined over Ω by proposition I. This implies $c(q^0_{i,j})$ is defined and upper bounded by a constant C.

Since $I^0_{i,j}$ is finite power signal over Ω, there exists an upper bound B such that $I^0_{i,j} < B$ for all $(i, j) \in \Omega$.

Therefore, we have $|div[c(q^0_{i,j})\nabla I^0_{i,j}]| \leq C|div[\nabla I^0_{i,j}]| = C(|\nabla^2 I^0_{i,j}|) \leq 4BC$.

Let Δt be chosen such that $\min\{I^0_{i,j}\} - (\Delta t/|\overline{\eta}_s|)4BC > 0$, i.e., $\Delta t < b/(BC)$, where $b \equiv \min\{I^0_{i,j}, (i, j) \in \Omega\}$. Then, we have $I^{\Delta t}_{i,j} > 0$ for any $(i, j) \in \Omega$. $I^{\Delta t}_{i,j}$ is upper bounded by$B + (\Delta t/|\overline{\eta}_s|)4BC$. From $I^0_{i,j}$ to $I^{\Delta t}_{i,j}$ we made the first iteration. Let $\Delta t(1)$ denote the chosen Δt for this iteration.

Step 2. Assume that at the nth iteration, the image $I^{\tau}_{i,j}$ is finite power signal and has no zero point everywhere, where $\tau = \sum_{m=1}^{n-1} \Delta t(m)$ with $\Delta t(m)$ being the time step for the mth iteration. From the result of step 1, there exists a $\Delta t(n)$ such that $I^{\tau+\Delta t(n)}_{i,j}$ is finite and has is supported (nonzero) over Ω.

If assigning $\Delta t = \min\{\Delta t(i)|i = 1, 2, \ldots\}$, then we know that (21) evolves without creating zeros. Q.E.D.

B. Speckle Removing Anisotropic Diffusion

1) Basic Theory: Based on previous discussion, we propose a new anisotropic diffusion method for smoothing speckled imagery. Given an intensity image $I_0(x, y)$ having finite power and no zero values over the image support Ω, the output image $I(x, y;\ t)$ is evolved according to the following PDE:

$$\begin{cases} \partial I(x, y;\ t)/\partial t = div[c(q)\nabla I(x, y;\ t)] \\ I(x, y;\ 0) = I_0(x, y),\ (\partial I(x, y;\ t)/\partial \vec{n})|_{\partial\Omega} = 0 \end{cases} \tag{32}$$

where $\partial\Omega$ denotes the border of Ω, $\vec{n}$ is the outer normal to the $\partial\Omega$, and

$$c(q) = \frac{1}{1 + [q^2(x, y;\ t) - q_0^2(t)]/[q_0^2(t)(1 + q_0^2(t))]} \tag{33}$$

or

$$c(q) = \exp\{-[q^2(x, y;\ t) - q_0^2(t)]/[q_0^2(t)(1 + q_0^2(t))]\}. \tag{34}$$

In (33) and (34), $q(x, y;\ t)$ is the instantaneous coefficient of variation determined by

$$q(x, y;\ t) = \sqrt{\frac{(1/2)(|\nabla I|/I)^2 - (1/4^2)(\nabla^2 I/I)^2}{[1 + (1/4)(\nabla^2 I/I)]^2}} \tag{35}$$

and $q_0(t)$ is the speckle scale function. We call (32) the SRAD PDE.

In the proposed SRAD, the instantaneous coefficient of variation $q(x, y;\ t)$ serves as the edge detector in speckled imagery. The function exhibits high values at edges or on high-contrast features and produces low values in homogeneous regions. The diffusion coefficient expressions in (33) and (34) follow the basic form of (2) and (3), respectively. The modification reflects encouraging isotropic diffusion in homogeneous regions of the image where $q(x, y;\ t)$ fluctuates around $q_0(t)$. Similar to the parameter k in (2) and (3), the speckle scale function $q_0(t)$ effectively controls the amount of smoothing applied to the image by SRAD. It is estimated using

$$q_0(t) = \frac{\sqrt{\mathrm{var}[z(t)]}}{\overline{z(t)}} \tag{36}$$

where $\mathrm{var}[z(t)]$ and $\overline{z(t)}$ are the intensity variance and mean over a homogeneous area at t, respectively.

2) Analytical Form of Scale Function $q_0(t)$: Because of the need of computing (36), the SRAD requires knowing a homogeneous area inside the image being processed. Although it is not difficult for a user to select a homogeneous area in the image, it is nontrivial for a computer. So, automatic determination of $q_0(t)$ is desired in real applications to eliminate heuristic parameter choice.

First of all, we state that $q_0(t)$ can be approximated by

$$q_0(t) \approx q_0 \exp[-\rho t] \tag{37}$$

where ρ is a constant, and q_0 is the speckle coefficient of variation in the observed image. For fully developed speckle, $q_0 = 1$ for ultrasound intensity data (without compounding) and $q_0 = 1/\sqrt{N}$ for N-look SAR intensity data. For partially correlated speckle, q_0 is less than unity.

Now, we give the derivation of (37). As we expected, in a uniform area the diffusion should be isotropic. Adopting the discrete isotropic diffusion update, we have

$$I^{t+\Delta t}_{i,j} = I^t_{i,j} + \frac{\Delta t}{4}\,(I^t_{i+1,j} + I^t_{i-1,j} + I^t_{i,j+1} + I^t_{i,j-1} - 4I^t_{i,j}). \tag{38}$$

Given $\sigma(t)$, the standard deviation of $I^t_{i,j}$ in a homogeneous region, we can estimate the standard deviation of $I^{t+\Delta t}_{i,j}$in the

region. Assuming that pixels in the region are statistically independent and identically distributed, we have from (38) and statistical formula for the variance of a sum of random variables

$$\sigma(t+\Delta t) = \sqrt{(1-\Delta t)^2\sigma^2(t) + (\Delta t/4)^2 4\sigma^2(t)}. \quad (39)$$

On the other side, the local means remains the same before and after an iteration. So, we have

$$q_0(t+\Delta t) = q_0(t)\sqrt{(1-\Delta t)^2 + (\Delta t)^2/4}. \quad (40)$$

For $\Delta t \ll 1$, the $(\Delta t)^2$ terms in (40) can be neglected, and we have

$$\sqrt{1-2\Delta t} \approx 1 - \Delta t \quad (41)$$

by Taylor series expansion and neglecting the second and higher order terms. So, (40) becomes

$$q_0(t+\Delta t) - q_0(t) + q_0(t)\Delta t \approx 0. \quad (42)$$

Dividing both sides of (42) by Δt, and taking limit as $\Delta t \to 0$, we have

$$\dot{q}_0(t) + q_0(t) \approx 0 \quad (43)$$

where $\dot{q}_0(t)$ is the first derivative of $q_0(t)$ with respect to t. Solving (43), yields

$$q_0(t) \approx q_0 \exp[-t]. \quad (44)$$

It is seen from (44) that through a diffusion process, speckle would be reduced exponentially (with a decay factor of 1) in homogeneous regions. We have observed that experimental curves of $q_0(t)$ appear as exponentially deceasing. However, the smoothing rate predicated by (44) is faster than those found in experiments.

The explanation for the insufficiency of (44) lies in the fact that (39) is correct only if all of $I^t_{i,j}$ values in a homogeneous region are truly independent at any t. Assume that the $I^0_{i,j}$ values in a homogeneous region are independent and identically distributed one-sided exponential random variables (as in the fully developed speckle case). As the iteration proceeds, the $I^t_{i,j}$ values will gradually become Gaussian random variables according to the central limit theorem. Meanwhile, the $I^t_{i,j}$ values become correlated as t increases. In general speckle cases, $I^0_{i,j}$ values may actually be correlated. So, the reduction rate of speckle variance in an iteration of diffusion should be smaller than that predicated by (44). This explanation suggests ways of modifying (44) for better agreement with experimental curves. One simple solution is changing (44) into (37) with a single constant $\rho(<1)$ being introduced to reduce the exponential decay rate. Fig. 1 shows the plots of $q_0(t)/q_0$ in which the solid line is predicated by (37) with $\rho = 1/6$, and the dashed line represents the experimental results computed using (36) within simulated ultrasonic image of carotid artery (see Results section). Given q_0 and ρ, and using (37) instead of (36) in implementing SRAD, the user does not have to choose a homogeneous region in the image.

C. Closer Look at SRAD

SRAD has some characteristics that are not shared with conventional anisotropic diffusion. We examine two of them here.

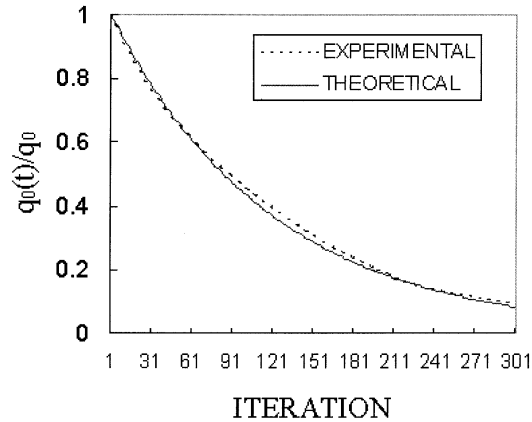

Fig. 1. Plots of $q_0(t)/q_0$ versus iteration.

For clarity, we write (32) as the sum of an isotropic term and an anisotropic term

$$\frac{\partial I}{\partial t} = c(q)\nabla^2 I + qc'(q)F \quad (45)$$

where $c'(x)$ is the first derivative of $c(x)$ and

$$F = \frac{1}{q}(q_x I_x + q_y I_y) \quad (46)$$

where $q_x = \partial q/\partial x$, $q_y = \partial q/\partial y$, $I_x = \partial I/\partial x$, and $I_y = \partial I/\partial y$.

First, let us consider the behavior of SRAD in homogeneous regions. Using (33), we know that $q \approx q_0(t)$, $c(q) \approx 1$ and $c'(q) \neq 0$. Since $c'(q) \neq 0$, at first glance, SRAD seems to be anisotropic even in homogeneous regions. However, recall that a homogeneous region is where the speckle is well developed. This implies that the fluctuation of values of pixels in uniform areas is highly random in space, leading to the spatial average of F over any microscopic zone is zero. So, macroscopically, the anisotropic term has no accumulative influence, yielding isotropic diffusion in homogeneous regions.

Then, we examine the behavior of (45) near an image edge. Let the edge direction η be the unit vector $[u, v]$. Let ξ denote the contour direction—the direction perpendicular to η, i.e., $\xi = [-v, u]$. Let $I_{\eta\eta}$ and $I_{\xi\xi}$ denote the second-order directional derivatives in the direction of η and ξ. The second-order derivatives along the η and ξ are computed as follows:

$$\begin{aligned} I_{\eta\eta} = {} & I_{xx}u^2 + I_{yy}v^2 + 2I_{xy}uv + [(u^2)_x/2 + vu_y]I_x \\ & + [(v^2)_y/2 + uv_x]I_y \end{aligned} \quad (47)$$

$$\begin{aligned} I_{\xi\xi} = {} & I_{xx}v^2 + I_{yy}u^2 - 2I_{xy}uv + [(v^2)_x/2 - uv_y]I_x \\ & + [(u^2)_y/2 - vu_x]I_y \end{aligned} \quad (48)$$

where $u_x = \partial u/\partial x$, $u_y = \partial u/\partial y$, $v_x = \partial v/\partial x$, $v_y = \partial v/\partial y$, and I_{xx}, I_{xy}, and I_{yy} are second derivatives of I.

The anisotropic term in (45) is driven by edges. So, the induced diffusion flow is in the edge direction. Let

$$I_{\eta\eta} = F. \quad (49)$$

Then, in the $\eta - \xi$ coordinates, equation (45) becomes

$$\frac{\partial I}{\partial t} = c(q)\left\{\left[1 + \frac{qc'(q)}{c(q)}\right] I_{\eta\eta} + I_{\xi\xi}\right\}. \quad (50)$$

Using (33), we can reduce (50) to

$$\frac{\partial I}{\partial t} = c(q)\left\{\left[\frac{1-q^2/q_0^4(t)}{1+q^2/q_0^4(t)}\right] I_{\eta\eta} + I_{\xi\xi}\right\}. \tag{51}$$

Since $q_0(t) \leq 1$ and $q \gg q_0(t)$ at an edge, we have that$[(1-q^2/q_0^4(t))/(1+q^2/q_0^4(t))] \approx -1$ near edges. This fact has a strong impact on SRAD. At the center of an edge, since $I_{\eta\eta}$ undergoes zero crossing, the SRAD diffusion proceeds only along the contour direction, just as with conventional anisotropic diffusion. However, on either side of an edge, "negative" diffusion occurs along the edge direction. This phenomenon in SRAD has not been observed with anisotropic diffusion, where the diffusion in the edge direction is gradually suppressed as approaching the edge center from either side of an edge. It is this "negative" diffusion that makes the dark side of edge darker and bright side of an edge brighter, leading to a sharper edge contour. Our experiments confirm the mean-preserving behavior in homogeneous regions and edge preserving and enhancement behavior at edges.

D. Discretization

The differential equation (32) may be solved numerically using an iterative Jacobi method. Assuming a sufficiently small time step size of Δt and sufficiently small spatial step size of h in x and y directions, we discretize the time and space coordinates as follows:

$$\begin{aligned} t &= n\Delta t, \qquad n = 0, 1, 2, \ldots \\ x &= ih, \qquad i = 0, 1, 2, \ldots, M-1 \\ y &= jh, \qquad j = 0, 1, 2, \ldots, N-1 \end{aligned}$$

where $Mh \times Nh$ is the size of the image support.

Let $I_{i,j}^n = I(ih, jh, n\Delta t)$. We then use a three-stage approach [7] to calculate the right hand side of the SRAD PDE. In the first stage, we calculate the derivative approximations and the Laplacian approximation as

$$\nabla_R I_{i,j}^n = \left[\frac{I_{i+1,j}^n - I_{i,j}^n}{h}, \frac{I_{i,j+1}^n - I_{i,j}^n}{h}\right] \tag{52}$$

$$\nabla_L I_{i,j}^n = \left[\frac{I_{i,j}^n - I_{i-1,j}^n}{h}, \frac{I_{i,j}^n - I_{i,j-1}^n}{h}\right] \tag{53}$$

$$\nabla^2 I_{i,j}^n = \frac{I_{i+1,j}^n + I_{i-1,j}^n + I_{i,j+1}^n + I_{i,j-1}^n - 4I_{i,j}^n}{h^2} \tag{54}$$

with symmetric boundary conditions

$$I_{-1,j}^n = I_{0,j}^n, \qquad I_{M,j}^n = I_{M-1,j}^n, \qquad j = 0, 1, 2, \ldots, N-1 \tag{55}$$

$$I_{i,-1}^n = I_{i,0}^n, \qquad I_{i,N}^n = I_{i,N-1}^n, \qquad i = 0, 1, 2, \ldots, M-1. \tag{56}$$

In the second stage, we calculate the diffusion coefficient $c(q)$ [see (33) and (34)] according to

$$c_{i,j}^n = c\left[q\left(\frac{1}{I_{i,j}^n}\sqrt{|\nabla_R I_{i,j}^n|^2 + |\nabla_L I_{i,j}^n|^2}, \frac{1}{I_{i,j}^n}\nabla^2 I_{i,j}^n\right)\right]. \tag{57}$$

Within the third stage, we calculate the divergence of $c(\cdot)\nabla I$, needed for the SRAD PDE in (32), as

$$\begin{aligned} d_{i,j}^n = \frac{1}{h^2}[&c_{i+1,j}^n(I_{i+1,j}^n - I_{i,j}^n) + c_{i,j}^n(I_{i-1,j}^n - I_{i,j}^n) \\ &+ c_{i,j+1}^n(I_{i,j+1}^n - I_{i,j}^n) + c_{i,j}^n(I_{i,j-1}^n - I_{i,j}^n)] \end{aligned} \tag{58}$$

with symmetric boundary conditions

$$d_{-1,j}^n = d_{0,j}^n, \qquad d_{M,j}^n = d_{M-1,j}^n, \qquad j = 0, 1, 2, \ldots, N-1 \tag{59}$$

$$d_{i,-1}^n = d_{i,0}^n, \qquad d_{i,N}^n = d_{i,N-1}^n, \qquad i = 0, 1, 2, \ldots, M-1. \tag{60}$$

Finally, by approximating time derivative with forward differencing, the numerical approximation to the differential equation is given by

$$I_{i,j}^{n+1} = I_{i,j}^n + \frac{\Delta t}{4} d_{i,j}^n. \tag{61}$$

Equation (61) is called the *SRAD update function*. With the SRAD update function in hand, we now demonstrate the efficacy of SRAD using (32) in terms of preserving the intra-region mean, reducing the intra-region variance, and preserving the edge positions. In numerical implementation, we choose $h = 1$ and $\Delta t = 0.05$; moreover, since the diffusion coefficient will not be exactly equal to zero at any edge in a digital image, as an option, we may set $c_{i,j}^n$ to be zero if it is less than a lower threshold T, to better stop diffusion across main edges.

IV. Experiments and Results

In this section, we test the SRAD PDE using both simulated and real ultrasound data. Additionally, we demonstrate the algorithm with real SAR data. First, we describe computer simulation of ultrasonic data. Then, we conduct three experiments using synthetic ultrasound images. In each experiment, we compare the results of the SRAD with those of three existing schemes, i.e., the enhanced Lee filter [12], the enhanced Frost filter [12], and anisotropic diffusion [15] applied as a homomorphic filter. We examine the mean preservation error and the standard deviation reduction to quantify the performance of algorithms in homogeneous regions. To compare edge preservation performance, we use Pratt's figure of merit [16]. Finally, we present two filtering results using real ultrasonic data and SAR data. So, the synthetic experiments allow the computation of ground truth information and thus the quantification of algorithm performance. The real image examples show the usefulness of SRAD for actual image processing applications using acquired data.

A. Simulation of Ultrasound Imagery of Carotid Artery

Let $V(x, y)$ represent a 2-D ultrasonic echo data set, where x and y denote axial and lateral coordinates, respectively. $V(x, y)$ is a bandpass signal in the axial direction. It is assumed that the imaging system has a linear, space-invariant point spread function. Allowing the population of scatterers of an object being

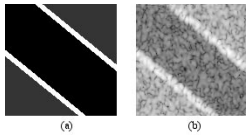

Fig. 2. Simulated data (a) backscatter cross section distribution (b) simulated image (imaging parameters: $f_0 = 10$ MHz, $\sigma_x = 2$, and $\sigma_y = 1.5$).

imaged to be represented by a scattering function, $T(x, y)$, the raw ("RF") data is governed by [4]

$$V(x, y) = h(x, y) * T(x, y) \tag{62}$$

where $*$ denotes spatial convolution. $T(x, y)$ accounts for acoustic impedance inhomogeneities in the object due to density and speed perturbation that generates the scattering, and $h(x, y)$ is the point spread function or impulse response of a hypothetical ultrasound imaging system. We assume that $h(x, y)$ is separable, i.e., $h(x, y) = h_1(x)h_2(y)$ where $h_1(x)$ is a Gaussian-weighted sinusoidal function (a Gabor function) determined by

$$h_1(x) = \sin(k_0 x)\exp[-x^2/(2\sigma_x^2)] \tag{63}$$

where $k_0 = 2\pi f_0/c$, c is the speed of sound in tissue, f_0 is the center frequency, and σ_x represents the pulse-width of transmitting ultrasonic wave. The second term $h_2(x)$ is the spatial response for the transmitting and receiving aperture determined by

$$h_2(x) = \exp[-y^2/(2\sigma_y^2)] \tag{64}$$

where σ_y represents the beam-width of transmitting ultrasonic wave. So, (62) can be computed by using two sequential 1-D convolutions: $V(x, y) = h_2(y) * h_1(x) * T(x, y)$.

A realistic biomedical model would include subresolution variations in object impedance from an average value. Therefore, in our test, we employ the following scattering model:

$$T(x, y) = t(x, y) \cdot G(x, y) \tag{65}$$

where $t(x, y)$ is the echogenicity model (or ultrasound cross section distribution) of the object being imaged, $G(x, y)$ is a Gaussian white noise field with zero mean and some variance. Specifically, a carotid artery echogenicity model for $t(x, y)$ is employed in our experiments as illustrated in Fig. 2(a). We chose the carotid artery as a prototypical experiment, because it is an application in which precise segmentation/boundary detection is required. The arterial wall thickness and the diameter of the artery reveal important parameters concerning diseases such as artheroschlerosis.

Since $V(x, y)$ is a bandpass signal, we express it in quadrature representation [1]

$$V_a(x, y) = V(x, y) + j\hat{V}(x, y) \tag{66}$$

where $\hat{V}(x, y)$ is the Hilbert transform of $V(x, y)$ with respect to x. Finally, we create an envelope-detected amplitude image (representing echo magnitude) given by

$$A(x, y) = |V_a(x, y)|. \tag{67}$$

TABLE I
CAROTID ARTERY MODEL PARAMETERS

Experiment No.	*B* Area I	*M* Area II	*W* Area III	*Var*	*Tilt*
I	1	5	20	1	≈45°
II	1	5	15	1	≈45°
III	1	5	20	2	≈45°

The simulated ultrasound image corresponding to Fig. 2(a) is shown in Fig. 2(b). The image is log-compressed for display, and the size of the image is 128 × 128 pixels.

B. Criteria for Quantifying Algorithm Performance

In our experiments, we are quantifying the algorithm performance in terms of edge preservation, mean preservation in a homogenous region and variance reduction in a homogeneous region.

1) Edge Preservation: To compare edge preservation performances of different speckle reduction schemes, we adopt the Pratt's figure of merit [16] defined by

$$FOM = \frac{1}{\max\left\{\hat{N}, N_{ideal}\right\}} \sum_{i=1}^{\hat{N}} \frac{1}{1 + d_i^2\alpha} \tag{68}$$

where $\hat{N}$ and N_{ideal} are the number of detected and ideal edge pixels, respectively, d_i is the Euclidean distance between the ith detected edge pixel and the nearest ideal edge pixel, and α is a constant typically set to 1/9. FOM ranges between 0 and 1, with unity for ideal edge detection.

FOM strongly depends on what method is used to obtain a binary edge map. Instead of using different edge detector that maximizes FOM for each despeckle scheme, we apply the same detector, the Canny detector [5], to provide a fair comparison of algorithms. To avoid oversmoothing due to the detector itself, we let the standard deviation of the Gaussian kernel in the Canny detector be $\sigma = 0.1$. Note that edge detection is performed on the processed intensity data, not upon the processed log compressed data (used for display). The ideal edges are extracted by applying the Canny detector with $\sigma = 4$ to the carotid artery model as shown in Fig. 2(a). The resulting ideal edges are close to manually delineated edges from the synthetic image.

2) Mean Preservation and Variance Reduction: The mean preservation and fluctuation reduction in homogeneous region are measures of success in terms of radiometric estimation. A successful speckle reducing filter will not significantly alter the mean intensity within a homogeneous region. Likewise, the effective speckle-reducing filter will reduce the variation within each homogeneous region. We compute and compare the mean and standard deviation over three different regions in our carotid artery simulation: within the artery, within the vessel wall and within fat/muscle regions.

C. Results

1) Simulation Results: Here, we present three sets of experimental results using three carotid artery echogenicity models that are parameterized as in Table I. In this table B, M and W denote the mean values of the ultrasound cross sections of

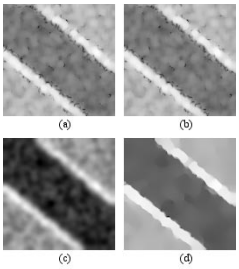

Fig. 3. (a)–(d) Filtered images using En-Lee, En-Frost., AD-Homomorph, and SRAD. In each case, the image displayed in Fig. 2(b) is the input image.

the artery interior, the muscle/fat region and the vascular wall, respectively. Var is the variance of the Gaussian fluctuation around mean cross sections, and *Tilt* denotes the orientation of the artery with respect to the horizontal direction.

Fig. 2(b) shows the simulated noisy image used in experiment I. Fig. 3 shows the smoothed images in experiment I, processed by using four speckle reduction schemes: enhanced Lee filter [12], enhanced Frost [12], anisotropic diffusion-based homomorphic filtering (denoted by "AD-homomorph" in the results), and SRAD, respectively. When applying the enhanced Lee filter (En-Lee) and enhanced Frost filter (En-Frost), the input data are intensity images, and the window sizes are set to 7×7 pixels. To compare SRAD to conventional anisotropic diffusion [15], we implemented diffusion in a homomorphic manner, since the conventional algorithm cannot eliminate multiplicative noise. The anisotropic diffusion-based homomorphic filtering is performed as follows: first we take the logarithmic transform of input data; then, we apply anisotropic diffusion [see (1) and (3)], and then compute the exponential point operation of the diffused data. In implementing the homomorphic anisotropic diffusion, we used a fixed number of iterations (=150) and a fixed time step (=0.1). To achieve the best results, we chose scaling factor $k = 3$ for synthetic data and SAR data, and $k = 5$ for real ultrasound data in (3). SRAD, in contrast, is applied directly to the intensity data. With SRAD, the diffusion coefficient is chosen as (33), the time step size is set to $\Delta t = 0.05$, and the number of iterations applied is 300.

Table II summarizes the mean preservation and variance reduction performance of the four filtering schemes in three experiments. In each experiment, the mean and standard deviations of three test areas are computed for each filtering scheme. The test areas are chosen in the artery interior (area I), the muscle/fat region (area II) and vessel wall region (area III).

Table III summarizes the edge preservation performance of the four filtering techniques in the three experiments.

These quantitative results show that the SRAD can eliminate speckle without distorting useful image information and without destroying the important image edges. In each experiment, SRAD outperformed the conventional speckle reducing filters and the conventional anisotropic diffusion algorithm in terms of edge preservation measured by the Pratt figure of merit. In nearly every case in every homogeneous region, SRAD produced the lowest standard deviation and were able to preserve the mean value of the region. The numerical results are further supported by qualitative examination (see Fig. 3, for example).

2) Real Image Results: A real ultrasonic image (128×128 pixels) of a human cartoid artery is shown in Fig. 4(a). The data was acquired using a LOGIQ 700 MR ultrasonic scanner manufactured by GE Medical Systems. During the data acquisition, the baseband complex echo signal was recorded. The real ultrasound image is taken as the amplitude of the baseband complex data set with time gating compensation for attenuation losses. Fig. 4(b)–(e) shows the smoothed images given by the four filters tested on the synthetic data. Note the smoothness of the homogeneous regions and the sharp, strong edges given by SRAD. The only negative feature of the SRAD result that is observable qualitatively is the slight broadening of the vessel walls. SRAD was implemented in Matlab (Mathworks, Natick, MA) and achieved a processing rate of 40 msec/iteration for a 128×128 image on a PC with a Pentium 4 (1.7 GHz) processor.

Fig. 5(a) shows a HH polarized 4-look SAR image of a central area in Hong Kong, China. The image data set was acquired by the NASA SIR-C L band polarimetric SAR system. Fig. 5(b)–(e) shows the smoothed images of the four filters when applied to the test data set. For AD-Homomorphic, and SRAD, the diffusion is stopped automatically when the residual error, defined as the mean square error of images between two iterations is smaller than 0.01.

From Fig. 5, it may be observed qualitatively that the conventional anisotropic diffusion cannot preserve salient features in the presence of speckle. The En-Lee filter and the En-Frost do reduce speckle but blur details. The proposed technique, SRADs gives the best performance in terms of smoothing noise and preserving edges at various scales. This SAR example is a dramatic exhibition of the improvement made possible by the PDE approach.

For all the results shown in Fig. 5(b)–(e), it appears that the linear features at the bottom of the image in Fig. 5(a) have been markedly degraded or lost. Essentially, features at the same scale as the speckle will be eliminated by all of the speckle reducing algorithms shown (Lee, Frost, SRAD) and will be also degraded by the conventional diffusion algorithm. The major region boundaries, however, are preserved, especially by the SRAD technique. Although this processed SAR result is purely qualitative, it shows promise for SRAD as a general-purpose speckle reducing filter.

V. Conclusions

In this paper we have developed a nonlinear anisotropic diffusion technique, speckle reducing anisotropic diffusion, for removing multiplicative noise in imagery. Unlike other existing diffusion techniques [2] that process log-compressed data, our technique processes the data directly in order to preserve useful information in the image. We have shown that with a special window, both the Lee filter and the Frost filter (which are commonly used for filtering SAR imagery) can be cast into the framework of a diffusion method. This observation has directed us to formulate a new adaptive edge-preserving PDE (in continuous image domain) tailored to speckled imagery. The SRAD PDE exploits the instantaneous coefficient of variation in reducing speckle. The performance figures obtained by means

TABLE II
MEAN AND STANDARD DEVIATION FOR UNIFORM REGIONS

Experiment I	Area I		Area II		Area III	
	Mean	Std.	Mean	Std.	Mean	Std.
Noisy image	1.0271	0.5605	5.3025	2.6896	22.7993	10.6100
En-Lee	1.1110	0.3227	5.7238	1.4223	21.7544	5.3673
En-Frost	1.1164	0.3207	5.7417	1.4066	21.8316	5.3034
AD-Homomorph	0.9009	0.2023	4.6416	1.0948	14.6472	3.5148
SRAD	1.1914	0.1470	6.1739	0.6957	18.8888	2.8543
Experiment II	**Area I**		**Area II**		**Area III**	
	Mean	**Std.**	**Mean**	**Std.**	**Mean**	**Std.**
Noisy image	1.0202	0.5585	5.2468	2.7187	14.3283	7.4439
En-Lee	1.1019	0.3301	5.6991	1.3541	13.9513	3.5778
En-Frost	1.1054	0.3263	5.7185	1.3412	14.0347	3.5354
AD-Homomorph	0.8887	0.2266	4.6019	0.8944	9.5239	1.9055
SRAD	1.1624	0.1632	6.0765	0.4165	12.9034	2.4012
Experiment III	**Area I**		**Area II**		**Area III**	
	Mean	**Std.**	**Mean**	**Std.**	**Mean**	**Std.**
Noisy image	1.2289	0.6697	5.5649	2.9400	20.2824	10.7690
En-Lee	1.3339	0.3671	6.0814	1.4934	19.6820	4.9464
En-Frost	1.3391	0.3652	6.0972	1.4827	19.7429	4.8886
AD-Homomorph	1.0729	0.2261	4.8765	1.0793	13.2277	2.8778
SRAD	1.4101	0.1531	6.4900	0.6902	17.6416	2.9878

TABLE III
PRATT'S FIGURE OF MERIT

	Experiment I	Experiment II	Experiment III
Image	***FOM***	***FOM***	***FOM***
Noisy	0.3072	0.3026	0.3002
En-Lee (7x7 window)	0.4632	0.4034	0.4591
En-Frost (7x7 window)	0.4574	0.4243	0.4592
AD-Homomorph	0.4714	0.4588	0.4909
SRAD	0.7257	0.6841	0.6958

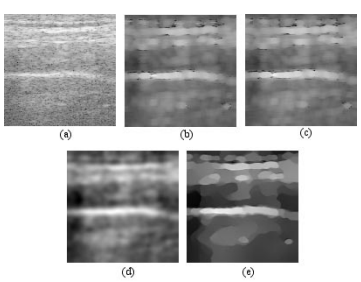

Fig. 4. (a) Original noisy image. (b)–(e) Filtered images from En-Lee, En-Frost, AD-Homomorph, and SRAD.

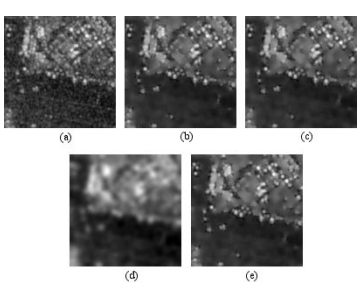

Fig. 5. (a) Original 125 × 125 SIR C SAR L-band HH image. (b)–(e) Filtered images by the En-Lee, En-Frost, AD-Homomorph, and SRAD filters.

of computer simulation reveal that the SRAD algorithm provides superior performance in comparison to the conventional anisotropic diffusion, the enhanced Lee filter and the enhanced Frost filter, in terms of smoothing uniform regions and preserving edges and features. The effectiveness of the technique encourages the possibility of using the approach in a number of ultrasound and radar applications.

ACKNOWLEDGMENT

The authors thank Dr. W. F. Walker, K. Ranganathan, M. J. McAllister, and F. Viola of the Department of Biomedical Engineering at UVa, for the discussions on ultrasonic image simulation and for providing real ultrasonic data.

REFERENCES

[1] P. Abbott and M. Braun, "Simulation of ultrasound image data by a quadrature method," in *Proc. Eng. Phys. Sci. Med. Health Conf.*, vol. 209, Canberra, Australia, Oct. 1996.
[2] K. Z. abd-Elmoniem, Y. M. Kadah, and A. B. M. Youssef, "Real time adaptive ultrasound speckle reduction and coherence enhancement," in *Proc. ICIP 2000*, Vancouver, BC, Canada, Sept. 10–13, 2000, pp. 1106–1109.
[3] S. T. Acton, "Locally monotonic diffusion," *IEEE Trans. Signal Processing*, vol. 48, pp. 1379–1389, May 2000.
[4] J. C. Bambre and R. J. Dickinson, "Ultrasonic B-scanning: A computer simulation," *Phys. Med. Biol.*, vol. 25, no. 3, pp. 463–479, 1980.
[5] J. Canny, "A computational approach to edge detection," *IEEE Trans. Pattern Anal. Machine Intell.*, vol. PAMI-8, 1986.
[6] V. S. Frost, J. A. Stiles, K. S. Shanmugan, and J. C. Holtzman, "A model for radar images and its application to adaptive digital filtering of multiplicative noise," *IEEE Trans. Pattern Anal. Machine Intell.*, vol. PAMI-4, pp. 157–165, 1982.
[7] J. S. Jin, Y. Wang, and J. Hiller, "An adaptive nonlinear diffusion algorithm for filtering medical images," *IEEE Trans. Inform. Technol. Biomed.*, vol. 4, pp. 298–305, Dec. 2000.
[8] D. T. Kuan, A. A. Sawchuk, T. C. Strand, and P. Chavel, "Adaptive restoration of images with speckle," *IEEE Trans. Acoust., Speech, Signal Processing*, vol. ASSP-35, pp. 373–383, 1987.
[9] J. S. Lee, "Digital image enhancement and noise filtering by using local statistics," *IEEE Trans. Pattern Anal. Machine Intell.*, vol. PAM1-2, 1980.
[10] ——, "Refined filtering of image noise using local statistics," *Comput. Graph. Image Process.*, vol. 15, pp. 380–389, 1981.
[11] ——, "Speckle suppression and analysis for synthetic aperture radar," *Opt. Eng.*, vol. 25, no. 5, pp. 636–643, 1986.
[12] A. Lopes, R. Touzi, and E. Nezry, "Adaptive speckle filters and scene heterogeneity," *IEEE Trans. Geosci. Remote Sensing*, vol. 28, pp. 992–1000, 1990.

[13] A. Lopes, E. Nezry, R. Touzi, and H. Laur, "Structure detection and statistical adaptive speckle filtering in SAR images," *Int. J. Remote Sensing*, vol. 14, no. 9, pp. 1735–1758, 1993.
[14] E. P. Papadakis, "Medical ultrasound diagnostics," in *Ultrasound Instruments and Devices*. New York: Academic, 1999.
[15] P. Perona and J. Malik, "Scale space and edge detection using anisotropic diffusion," *IEEE Trans. Pattern Anal. Machine Intell.*, vol. 12, pp. 629–639, 1990.
[16] W. K. Pratt, *Digital Image Processing*. New York: Wiley, 1977.
[17] M. Sonka, X. Zhang, M. Siebes, M. S. Bissing, S. C. Dejong, S. M. Collins, and C. R. McKay, "Segmentation of intravascular ultrasound images: A knowledge-based approach," *IEEE Trans. Med. Imag.*, vol. 14, pp. 719–732, 1995.
[18] Z. Sun, H. Ying, and J. Lu, "A noninvasive cross-correlation ultrasound technique for detecting spatial profile of laser-induced coagulation damage—An *in vitro* study," *IEEE Trans. Biomed. Eng.*, vol. 48, pp. 223–229, Feb. 2001.
[19] G. E. Trahey, S. M. Hubbard, and O. T. von Ramm, "Angle independent ultrasonic blood flow detection by frame-to-frame correlation of B-mode images," *Ultrasonics*, vol. 26, pp. 271–276, 1988.
[20] G. E. Trahey, S. W. Smith, and O. T. von Ramm, "Speckle reduction in medical ultrasound via spatial compounding," in *Proc. SPIE Med. XIV PACS*, vol. 4, 1986, pp. 626–637.
[21] D. Y. Tsai and S. Watanabe, "A method for optimization of fuzzy reasoning by genetic algorithms and its application to discrimination of myocardial heart disease," *IEEE Trans. Nucl. Sci.*, vol. 46, pp. 2239–2246, Dec. 1999.
[22] J. Wang and X. Li, "A system for segmenting ultrasound images," in *Proc. 14th Int. Conf. Pattern Recognition*, vol. 1, 1998, pp. 456–461.
[23] S. H. Wong, K. L. Chan, and P. W. Fung, "Automatic segmentation of ultrasonic images," in *Proc. Computer, Communication, Control, Power Engineering (TENCON'93)*, vol. 2, IEEE Region 10 Conf., Part: 2, 1993, pp. 910–913.

Yongjian Yu was born in Sichuan, China, in 1961. He received the B.S. degree in physics and the M.S. and Ph.D. degrees in electrical engineering from University of Electronic Science and Technology of China (UESTC), Sichuan, in 1982, 1985, and 1989, respectively.

He was a member of the faculty of UESTC from 1989 to 1999, where he held the position of Associate Professor of electronic engineering 1993 to 1999. From August 1993 to December 1995, he was a Visiting Scholar with the Remote Sensing Group, Alenia Spazio SpA, Rome, Italy. From 1999 to 2000, he was a Research Assistant with the Department of Electrical and Computer Engineering, Oklahoma State University, Stillwater. Since 2000, he has been a Research Assistant with the Department of Electrical and Computer Engineering, University of Virginia, Charlottesville. His current research interests include ultrasound imaging, signal, image, and video processing system.

Dr. Yu received the Science and Technology Progress Award of the Ministry of Electronics Industry of China in 1994 and the National Scientific and Technological Progress Award of China in 1999.

Scott T. Acton (S'89–M'93–SM'99) received the B.S. degree in electrical engineering from Virginia Tech, Blacksburg, in 1988 as a Virginia Scholar. He received the M.S. degree in electrical engineering and the Ph.D. degree in electrical engineering from the University of Texas at Austin in 1990 and 1993, respectively.

He is currently an Associate Professor with the Department of Electrical and Computer Engineering, University of Virginia, Charlottesville. He has worked in industry for AT&T, the MITRE Corporation, and Motorola, Inc., and in academia for Oklahoma State University, Stillwater. His research interests include biomedical image analysis, multiscale signal representations, diffusion algorithms, active contours, video tracking, image morphology, image segmentation, and content-based image retrieval.

Dr. Acton is the winner of the 1996 Eta Kappa Nu Outstanding Young Electrical Engineer Award, a national award that has been given annually since 1936. He also received the 1997 Halliburton Outstanding Young Faculty Award. He has served as Associate Editor of the IEEE TRANSACTIONS ON IMAGE PROCESSING and is currently serving as Associate Editor of the IEEE SIGNAL PROCESSING LETTERS.